The Astrophysical Journal Supplement Series, 276:13 (9pp), 2025 January https://doi.org/10.3847/1538-4365/ad927a

Simulating a Steady-state Heliosphere

Jacob Heerikhuisen[1], Eric J. Zirnstein[2], and Nikolai V. Pogorelov[3]
[1] Department of Mathematics, University of Waikato, Hamilton, New Zealand; jacobh@waikato.ac.nz
[2] Department of Astrophysical Sciences, Princeton University, Princeton, NJ 08544, USA
[3] Department of Space Science, University of Alabama in Huntsville, Huntsville, AL 35899, USA

Received 2023 December 18; revised 2024 October 22; accepted 2024 November 12; published 2024 December 26

Abstract

Ever since the discovery of the solar wind, it has been understood that our solar system resides within a bubble of solar wind plasma that originates from the Sun. Due to its vast size, the geometry of this bubble, known as the heliosphere, remains a topic of conjecture and debate. Three-dimensional simulations, employing magnetohydrodynamics coupled to neutral particles, provide a key way of understanding the global flow dynamics on macroscopic scales. While many of these models suggest a comet-like shape with a single heliotail for the heliosphere, others have suggested geometries with two distinct outflows of solar wind plasma. In this paper we show how numerical simulations with the same boundary conditions may evolve differently, depending on factors such as initial conditions and run time. We find that the eventual steady state is the same comet-like shape, even for less than optimal choices of the initial condition.

Unified Astronomy Thesaurus concepts: Heliosphere (711); Heliopause (707); Astrosphere interstellar medium interactions (106)

1. Introduction

The heliosphere is the region of space encompassing and surrounding the solar system that is filled by the magnetic field and material originating from the Sun. The heliosphere is formed by the continuous outflow of plasma from the Sun, known as the solar wind (SW), and its interaction with the plasma present in our region of the Galaxy (E. N. Parker 1961; G. P. Zank 1999). The heliosphere is characterized by a supersonic outflow of SW from the Sun that becomes subsonic at the heliospheric termination shock (TS), whereupon it is deflected away from the impinging flow of the local interstellar medium (LISM). The SW and LISM plasmas are separated by a tangential discontinuity known as the heliopause (HP). As the Sun moves through the LISM, it leaves behind a trail of SW plasma, known as the "heliotail." Eventually, far downstream of the Sun, the SW and LISM flows equilibrate and merge.

While we have direct measurements of the front of the heliosphere from NASA's Voyager 1 and Voyager 2 spacecraft, both of which have crossed the TS (L. F. Burlaga et al. 2005, 2008; R. B. Decker et al. 2005, 2008; E. C. Stone et al. 2005, 2008) and HP (D. A. Gurnett et al. 2013; E. C. Stone et al. 2013; L. F. Burlaga & N. F. Ness 2014; D. A. Gurnett & W. S. Kurth 2019; S. M. Krimigis et al. 2019; J. D. Richardson et al. 2019), knowledge of the plasma flows behind the heliosphere remains less constrained by data. Early models of the heliosphere (E. N. Parker 1961; G. Yu 1974) showed that either one or two outflow channels, or heliotails, could be possible, depending on the parameters of the SW and LISM plasmas, and particularly their corresponding magnetic fields. Subsequent three-dimensional numerical simulations of the SW–LISM interaction showed that most realistic sets of parameters result in a single (or "comet-like") heliotail (e.g., T. J. Linde et al. 1998; N. V. Pogorelov & T. Matsuda 1998; T. Tanaka & H. Washimi 1999; N. V. Pogorelov et al. 2004; V. Izmodenov et al. 2005; M. Opher et al. 2006; N. V. Pogorelov et al. 2006; J. Heerikhuisen et al. 2008; R. Ratkiewicz & J. Grygorczuk 2008; O. Sternal et al. 2008). A study by S. Korolkov & V. Izmodenov (2021) suggests that a double-tailed astrosphere is possible for a range of stellar wind and ISM conditions, not only just in the limit of zero flow (E. N. Parker 1961; J. F. Drake et al. 2015; E. A. Golikov et al. 2017). The results of Korolkov & Izmodenov rule out a double-tailed solution for the heliosphere, since these are predicted to exist only for a subsonic LISM.

M. Opher et al. (2015, 2016) presented results from a simulation that show a double-tailed (or "croissant-like," M. Opher et al. 2016) heliosphere with two distinct outflows. While it was suggested that this may herald a new picture of the heliosphere (M. Opher et al. 2015), other groups were not able to reproduce this specific geometry, even using the same model parameters. In fact, N. V. Pogorelov et al. (2015) showed that the assumption in M. Opher et al. (2015) of a unipolar magnetic field for the Sun significantly enhances the magnetic field in the heliosheath, resembling the double-tailed structure suggested by G. Yu (1974), though the magnetic tube structures still result in a single heliotail. Those authors also point out that a kinetic treatment of neutrals and a time-dependent SW both prevent magnetic tube structures from developing, and hence a single tail is the most likely geometry for our heliosphere. Furthermore, N. V. Pogorelov et al. (2017) show that any signature of the split-tail configuration disappears if solar cycle effects are taken into account. Finally, E. J. Zirnstein et al. (2017) show that a time-dependent single-tailed heliosphere reproduces the heliotail lobe structure observed in energetic neutral atom maps from the IBEX spacecraft (D. J. McComas et al. 2013). We also note here that later versions of the model first shown in M. Opher et al. (2015), namely M. Kornbleuth et al. (2021) and A. T. Michael et al. (2022), do not display a strong croissant-like shape. M. Kornbleuth et al. (2021) show a good agreement between their heliosphere and one obtained using the Moscow Model (V. V. Izmodenov & D. B. Alexashov 2020),

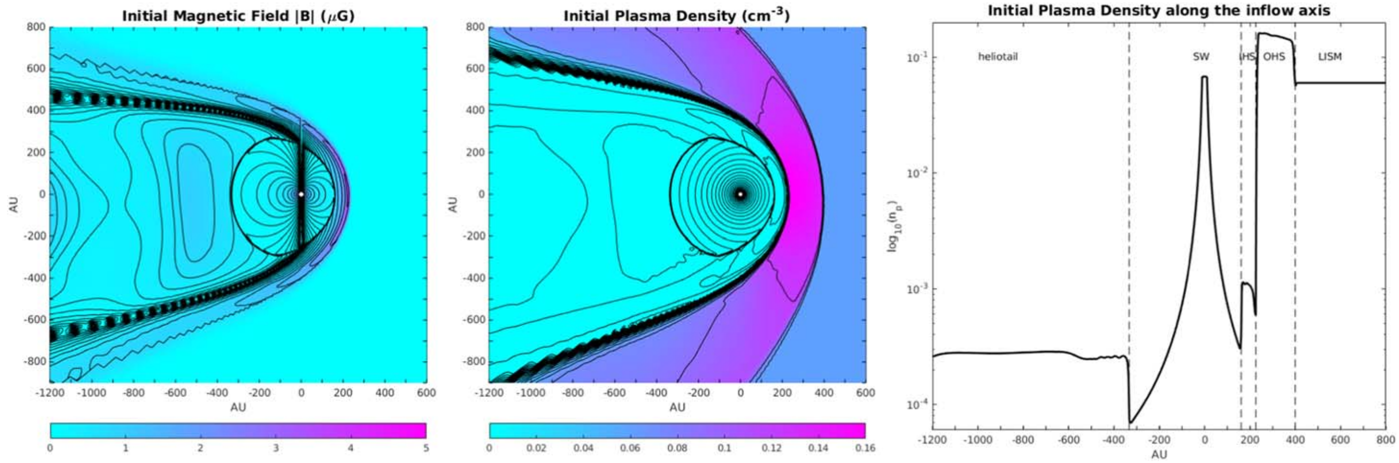

Figure 1. Meridional slices of the magnetic field magnitude (left) and proton density (middle) for the plasma configuration from which three of the plasma–neutral models start. In both plots the contour lines are computed on a logarithmic scale to highlight the geometry of the low-density and low magnetic field regions inside the heliosphere. The right-hand plot shows the plasma density along the LISM flow axis on a logarithmic scale.

except for transition between the SW and LISM plasmas (i.e., the HP), which the models handle differently. The work of A. T. Michael et al. (2022) is axially symmetric, necessitating a single heliotail, but the results compare well to other heliospheres (D. Alexashov & V. Izmodenov 2005; J. Heerikhuisen et al. 2006).

In this paper we show that a steady-state heliospheric simulation can transition from a single-tailed to a double-tailed structure by changing the initialization method, while keeping the boundary conditions the same. The resulting heliosphere resembles the two-tailed structure shown in M. Opher et al. (2015) after plasma–neutral coupling is initiated, though all our simulations eventually reach a single-tailed steady state. More generally, we show how a steady-state heliosphere can be obtained using variations on the commonly applied time-marching approach, and that certain strategies can speed up the convergence of the solution.

2. Model of the SW–LISM Interaction

We utilize a three-dimensional model of the SW–LISM interaction based on the MS-FLUKSS suite (N. V. Pogorelov et al. 2006; J. Heerikhuisen et al. 2008; R. K. Bera et al. 2023; F. Fraternale et al. 2023). For the runs considered here we solve the time-dependent magnetohydrodynamic (MHD) equations with source terms for charge exchange with neutral hydrogen (H. L. Pauls et al. 1995). The charge-exchange source terms are computed using a particle-based Monte Carlo (MC) code that solves the time-dependent Boltzmann equation and aggregates individual charge-exchange events occurring during a given time interval onto the grid of source terms (J. Heerikhuisen & N. V. Pogorelov 2010). The solution to the MHD–neutral system is obtained by applying SW boundary conditions near the Sun (on a 10 au sphere) and LISM conditions far from the Sun (on a 3000 au sphere).

When we apply this method to solve a time-dependent problem, we iterate between the MHD and MC solvers, letting each evolve the solution forward in time over some (short) time interval τ (E. J. Zirnstein et al. 2015). This allows us to address time-dependent problems with a time resolution as fine as $\tau \simeq 0.25$ yr (E. J. Zirnstein et al. 2015, 2017; D. J. McComas et al. 2018; E. J. Zirnstein et al. 2018). Higher time fidelity is possible using fluid neutrals (N. V. Pogorelov et al. 2013; T. K. Kim et al. 2016)

Although the SW leaving the Sun is highly dynamic on a multitude of timescales, these changes tend to average out over longer timescales and larger radial distances. The most significant changes in the SW occur over the 11 yr solar cycle, which can result in displacements of ∼10 au and ∼8 au for the TS and HP, respectively (N. V. Pogorelov et al. 2009; D. J. McComas et al. 2018; V. V. Izmodenov & D. B. Alexashov 2020; J. Kleimann et al. 2022; E. J. Zirnstein et al. 2022). If we are interested in the longer-term average configuration of the heliosphere, especially aspects like the HP location, the draping of LISM magnetic field around the heliosphere, and the geometry of the heliotail, we may fix the boundary conditions and look for a steady-state solution.

The traditional way to obtain a steady-state solution to this type of flow problem is to fix the boundary conditions and let the system relax to a steady state by solving the time-dependent problem. One issue with this approach is that if the flow is turbulent, a truly time-stationary state cannot be reached, and we instead approach an approximately steady-state solution. In practice such "time marching" to a steady state requires the system to run for timescales comparable to the time for the LISM to flow through the domain (∼1000 yr). Because the neutrals have large mean free paths (typically ∼100 au), small-scale structure in the plasma (e.g., turbulence) does not affect the neutrals in a significant way. For this reason, it is possible to run the neutral code for a longer time between iterations, which speeds up the convergence to a steady state. In the next section we discuss three simulation strategies.

2.1. Initial and Boundary Conditions

We run four versions of our MHD–neutral model of the heliosphere. Three of the four versions start from the same initial plasma configuration, obtained by running the model without neutrals. This configuration is shown in Figure 1. The first version of our heliospheric simulation (Model I) solves the plasma–neutral system by starting from a plasma configuration obtained without neutrals (i.e., a heliosphere without neutrals, Figure 1) and a neutrals configuration obtained without plasma (i.e., uniformly distributed LISM conditions). The MHD–neutral model is then run by solving the time-dependent

Table 1
Differences in Simulation Assumptions

Model	Iteration Times	Plasma Initial Condition	Neutral Initial Condition
I	1 yr for both plasma and neutrals	plasma-only heliosphere	fill with LISM properties
II	1 yr for plasma, 4000 yr for neutrals	plasma-only heliosphere	fill with LISM properties
III	1 yr for both plasma and neutrals	SW initiated at $r = 10$ au	fill with LISM properties
IV	1 yr for both plasma and neutrals	plasma-only heliosphere	LISM plus additional population

problem with $\tau = 1$ yr time iterations. This means the neutrals are run on the current plasma configuration for 1 yr, the resulting source terms are then applied to the MHD equations, which are then run for 1 yr. This process slowly moves the system to a steady-state configuration. In what follows, times quoted represent the time over which the plasma has evolved, where $t = 0$ is the initial condition (see also Table 1).

Model II tries to speed up the convergence to a steady state by running the neutrals for a much longer time (4000 yr) for each plasma–neutral iteration. Effectively this means the neutrals fully equilibrate with the current plasma configuration and produce source terms accordingly. The MHD module is still run for 1 yr for each set of source terms. In this case we use fewer computational neutral particles, but evolve them for a longer time, so that the overall run time for Model II is similar to Model I. The expectation is that this approach will speed up the convergence to a steady state since the neutrals are effectively in a steady state with respect to the plasma at all times.

Model III does not start from a plasma-only heliosphere. Instead we start from equilibrium LISM conditions for both plasma and neutrals. We then initiate the simulation by turning on the SW and by applying the SW boundary conditions on a 10 au sphere around the Sun. This inflates the heliosphere over time in the presence of neutrals, so that the size of the heliosphere never exceeds its final size.

Model IV represents a situation where the initial conditions are not as simple as the other three cases, and we instead introduce aspects of the expected steady-state solution. We know from simulations with multiple neutral fluids (e.g., J. Heerikhuisen et al. 2006) that upstream of the heliosphere we have both a primary population of neutrals with LISM properties, as well as a warmer population of “secondary” neutrals that are created through charge exchange just outside the HP. While these secondary neutrals will eventually end up with a complex spatially dependent flow profile, we can try to account for their eventual presence by including an additional population of neutrals as part of the initial condition. For Model IV we assume an additional population of neutrals of uniform density within a rectangular domain that extends to 600 au from the Sun in all directions, except the tail, where it extends to 1000 au. We assume that this population has a uniform bulk velocity of 15 km s^{-1} toward the upwind LISM. While most secondary neutrals will eventually flow in the downwind LISM direction, our choice is motivated by the flow velocity of secondary neutrals upstream of the bow shock (or bow wave). We choose the density of the additional population of neutrals to be the same as the LISM neutral density, since the steady-state density of primary and secondary neutrals are similar (J. Heerikhuisen et al. 2006). While it turns out that this particular choice actually slows the convergence, the key reason we include Model IV is to illustrate how a different (i.e., suboptimal) initialization can affect the way the solution evolves to a steady state, and also that it will eventually reach the same steady state as the other three models. The exact parameters used for all four models are outlined in Table 1.

Table 1 shows the different assumptions made in the four models we consider. For all models we assume the following LISM conditions: $n_p = 0.06$ cm^{-3}, $n_{\rm H} = 0.18$ cm^{-3}, $U = 26.4$ km s^{-1}, $T = 6500$ K, and $|B| = 0$. The interstellar magnetic field is set to zero, consistent with the simulations of M. Opher et al. (2015). The SW conditions at 1 au assumed in all four models are $B_r = 50$ μG, $n_p = 7.85$ cm^{-3}, $U = 420$ km s^{-1}, and $T = 100{,}000$ K. The coordinate system is defined such that the z-axis aligns with the solar magnetic and rotation axis. The x-axis points in the upstream LISM direction, such that the LISM flow vector lies in the XZ plane. Note that the ecliptic plane makes an angle of 7°25 with respect to the equatorial plane, with the line of nodes aligned close to the x-axis. The LISM flow vector makes an angle of 5°1 with the ecliptic plane, which translates to an angle of just over 5° to the x-axis. The y-axis completes the right-handed coordinate system. The magnetic field is outward in both the northern and southern hemispheres of the inner boundary, making the SW magnetic field unipolar. This assumption is sometimes used in simulations to avoid a current sheet that models cannot properly resolve (V. V. Izmodenov & D. B. Alexashov 2015; M. Opher et al. 2015; N. V. Pogorelov et al. 2015; M. Kornbleuth et al. 2021). Finally, the initial condition for Model IV includes an additional neutral population with properties $n_{\rm H,2} = 0.18$ cm^{-3}, $U_{\rm H,2} = 15$ km s^{-1}, $T_{\rm H,2} = 10{,}000$ K.

3. Results

As noted in Section 2, the four models we consider employ the same boundary conditions, so all four should approach the same steady state if we solve the time-dependent plasma–neutral system. In Figure 2 we show the magnetic field configuration after the plasma has evolved 200 yr from the initial configuration (shown in Figure 1 for Models I, II, and IV). It is immediately apparent that Models I, II, and III show a very similar single-tailed heliosphere, while Model IV appears “croissant” shaped. There are slight differences in the magnetic field between Models I, II, and III, where the configuration in Model II is smoother due to the charge-exchange source terms having been computed when the neutrals are in equilibrium with the plasma, while for the other models the neutrals do not reach such an equilibrium during each 1 yr neutral time step. The source terms in Model II are also a bit smoother because the longer accumulation time allows for better particle statistics. Although the boundary conditions for the four models set the LISM magnetic field to zero, the numerical scheme allows some of the SW magnetic field to dissipate across the HP. To avoid generating contour lines of the field outside the heliosphere we have only plotted them for the region of space inside the HP defined by the temperature

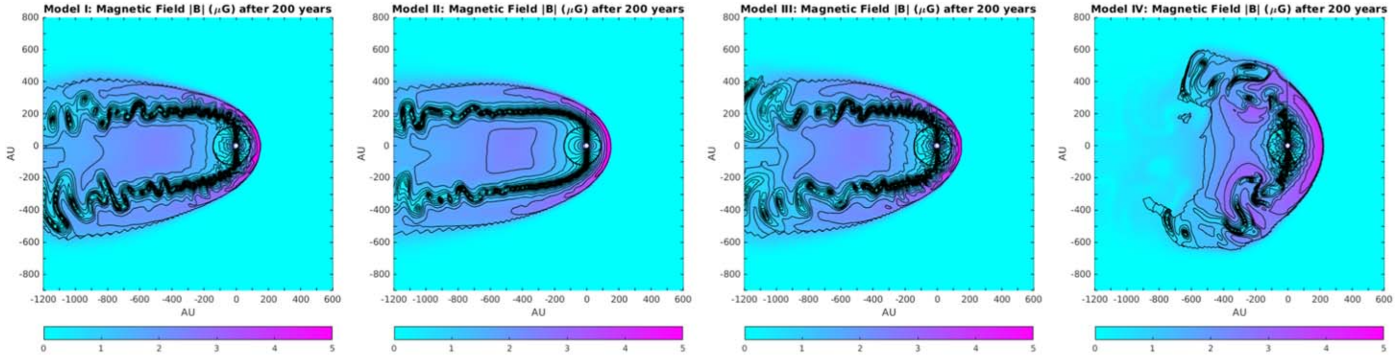

Figure 2. Meridional slices of the magnetic field magnitude for the four models considered, after the plasma has evolved for 200 yr from the initial condition. Here the color scale is linear, while contour lines have been added on a logarithmic scale to highlight the geometry of the weaker field emanating from the polar regions of the Sun.

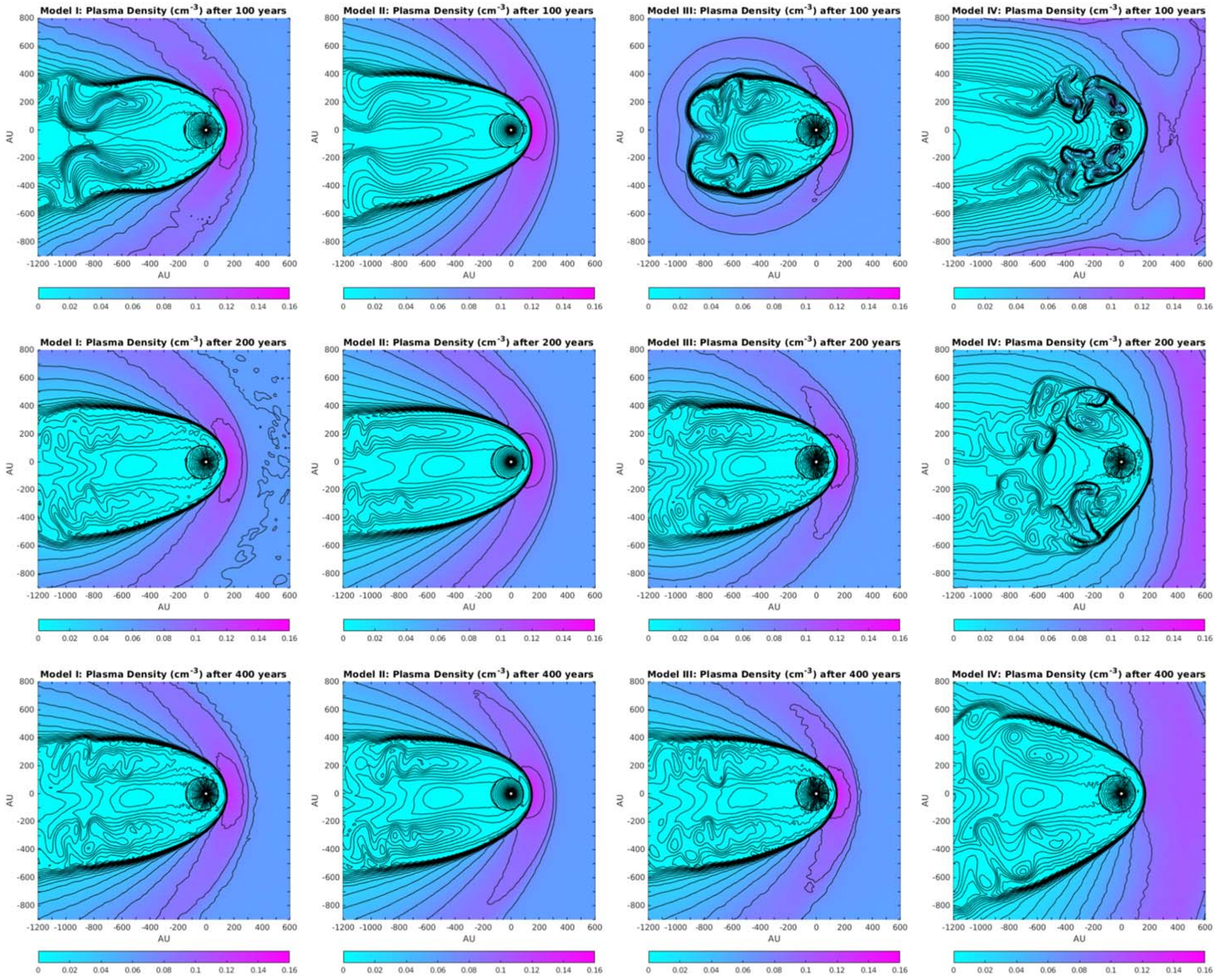

Figure 3. Meridional slices of the proton density for the four models considered, after the plasma has evolved for 100 yr (top row), 200 yr (middle row), and 400 yr (bottom row) from the initial condition. Here the color scale is linear, while contour lines have been added on a logarithmic scale to highlight the geometry of the low-density region downstream of the heliosphere.

isosurface $T = 40{,}000$ K. In Section 4 we will look more closely at strategies for defining the HP.

Figure 3 shows the density for the four models at 100, 200, and 400 yr after the initial condition. After 100 yr, Models I and II show the effect of charge exchange in shrinking the heliosphere when compared to the initial condition (shown in Figure 1). The subsequent 100 yr only evolve the heliosphere slightly, with the biggest changes occurring in the heliotail

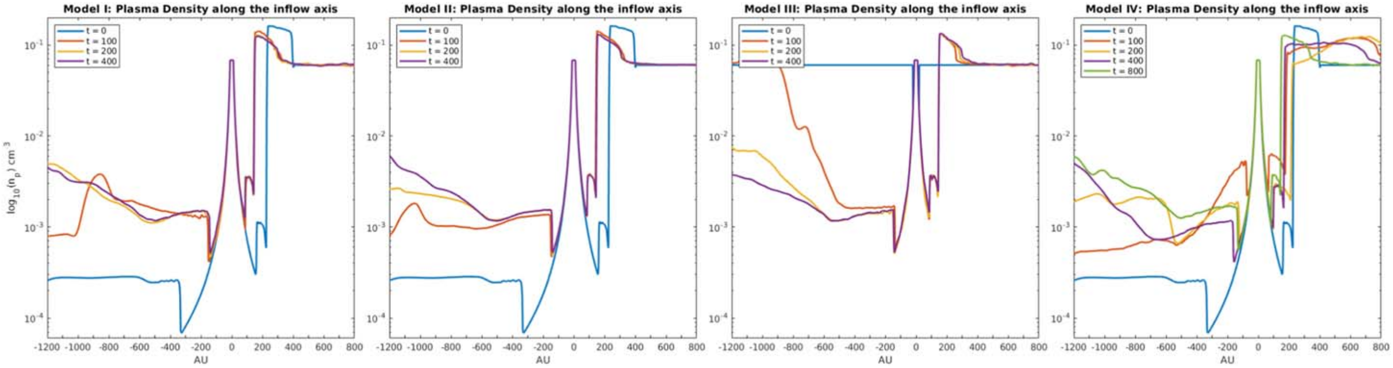

Figure 4. Proton density along the LISM flow axis for the four models considered, taken at different times after the initial condition. Here Models I–III have converged after 400 yr, while Model IV needs at least another 400 yr to reach the same steady state.

region. The inflation of the heliosphere, following its initiation at time zero, can be seen in the plot for Model III. After 200 yr this Model already closely resembles Models I and II, though its downstream boundary continues to expand (see also Figure 4). The presence of an additional population of neutrals in the initial condition causes significantly more charge exchange during the first 100 yr for Model IV, compared to Models I, II, and III. This results in a much smaller TS, and a slowing of the plasma in the inner heliosheath leading to higher density and a turbulent flow. Model IV shows a significant growth phase after 100 yr, so that by 200 yr the heliosphere extends much farther in the polar directions than the other two models. The bottom row of Figure 3 shows that models I–III have reached the same steady-state configuration, while Model IV still shows the effects of its suboptimal initial condition.

To get a better sense of the time evolution in the four models, in Figure 4 we plot plasma density along cuts through the domain that include the Sun and run parallel to the LISM flow direction. For each model we plot the density at times $t = 0$, 100, 200, 400 yr after the initial condition, and for Model IV we also include $t = 800$ yr. For Models I and II the TS and HP move inward after neutrals are introduced, and the smaller heliosphere results in a higher density for the outflow along the heliotail. Conversely, the heliosphere in Model III starts from a uniform LISM density, and the low-density (high-pressure) plasma of the SW carves out the heliosphere, reaching a similar profile to Models I and II after 400 yr. Clearly the additional population of neutrals introduced in Model IV initially shrinks the TS and HP after 100 yr, but then temporarily expands the HP back before finally settling into the same steady-state solution as Models I–III. Note how in Model II the solution after 200 yr is almost indistinguishable from the one after 400 yr from upstream of the heliosphere to about 700 au down the heliotail, adding weight to the idea that allowing the neutrals to equilibrate fully at each plasma step leads to more rapid convergence to a steady state. Interestingly it seems that the longer neutral run times of Model II may in fact slow the convergence of the solution in the distant ($\gtrsim$700 au) heliotail.

4. The Heliopause

We know from theory, and we see from simulations, that the SW–LISM interaction always includes a tangential discontinuity, known as the HP, where the total pressure of the SW balances that of the LISM. In the upwind direction of the LISM, the HP transition is accompanied by around a 50-fold increase in density, as measured by the Voyagers (D. A. Gurnett & W. S. Kurth 2019; W. S. Kurth & D. A. Gurnett 2020), and also observed in MHD–neutral models of the SW–LISM interaction (e.g., J. Heerikhuisen et al. 2014; V. V. Izmodenov & D. B. Alexashov 2015; N. V. Pogorelov et al. 2017). In simulations, a jump in the total plasma temperature is often used to identify the HP (e.g., S. N. Borovikov et al. 2008; J. Heerikhuisen et al. 2014; M. Opher et al. 2015; E. J. Zirnstein et al. 2018), though the temperature and density jumps are similar since total pressure is constant across the HP.

Figure 5 shows temperature contours for Models I–IV that may be used to estimate the location of the HP. Here we see that for the front of the heliosphere all of the temperature contours almost lie on top of each other, suggesting that they all trace out the shape of the heliosphere in this region. In the heliotail region the hot plasma produced at the TS cools with distance as cold neutrals from the LISM undergo charge exchange and remove energy from the SW. Interestingly Model II has a hotter tail at this time (200 yr after the initial condition), which is due to hot neutrals (i.e., energetic neutral atoms) created near the TS having time, due to this model's long neutral iterations, to charge exchange and deposit their energy in the distant heliotail. Figure 6 shows the same temperature contours once the models have reached their steady state. At this time in the simulations any of the temperature contours still represent a good approximation to the HP in the front half of the heliosphere. The similarity between the plots also shows that at this time (400 yr for Models I–III, and 800 yr for Model IV) the solutions are effectively the same.

While using a single isosurface of temperature to locate the HP in simulations is convenient, the accuracy of this approach breaks down in the heliotail, where the level surface does not correspond to the HP. At best, the isosurface represents a single point within a layer of high temperature gradient, and so various temperature levels could be used that provide different locations for the HP. A more robust approach is to trace streamlines, though these are only valid in a true steady state. Alternatively, a passive tracer can be embedded in the flow (S.N. Borovikov et al. 2011; S. Korolkov & V. Izmodenov 2021) with, for example, the value 1 at the SW boundary and value −1 at the LISM boundary. The HP would then be defined at the zero surface of this tracer. In practice, diffusion and mixing occurs and the HP surface will be smeared over several grid cells. This problem is typically solved by periodic reinitialization of the level-set function (S. Osher & R. P. Fedkiw 2001; S.N. Borovikov et al. 2011).

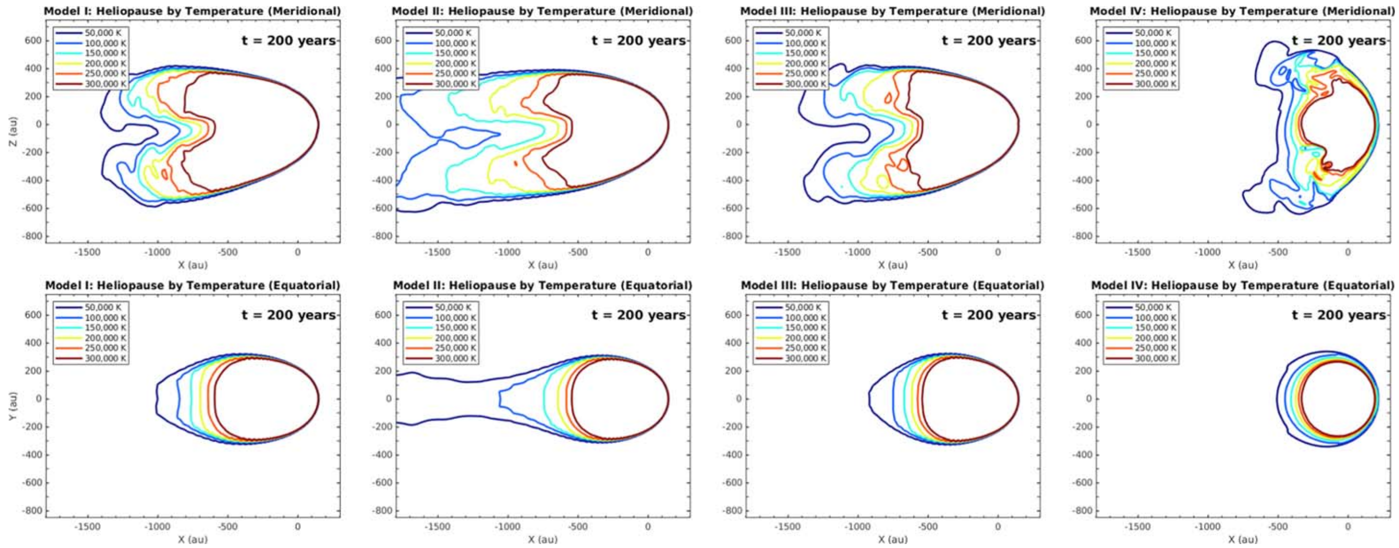

Figure 5. Contours of plasma temperature in the solar equatorial plane (bottom row) and meridional plane (top row) taken 200 yr after the initial condition.

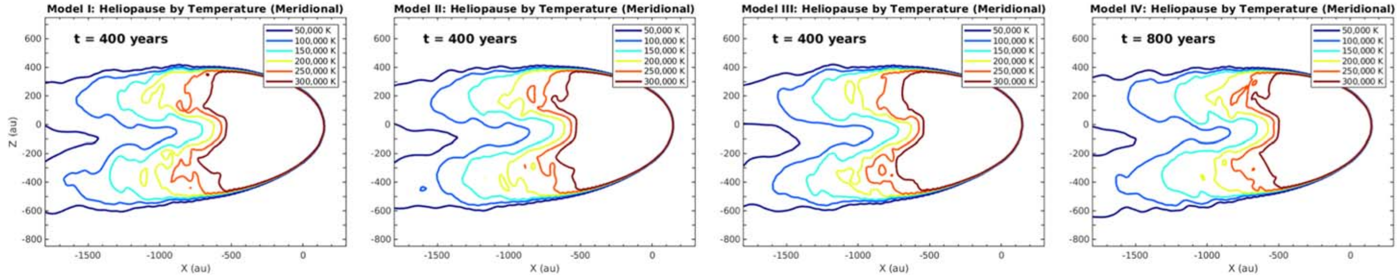

Figure 6. Contours of plasma temperature in the solar equatorial plane after 400 yr (Models I–III) and 800 yr (Model IV). By this time all four models have reached the same steady-state configuration.

An alternative approach we propose here involves looking for several defining properties of the HP in the solution. By definition all flow is parallel to the HP, and in the case of the heliosphere, there is a jump in both density and temperature across the surface. The method involves computing the gradient of either the density or temperature, and looking at locations where the magnitude of its component perpendicular to the flow is a local maximum. In practice we find that using density provides slightly nicer results, and the quantity we plot is

$$g(\boldsymbol{r}) = \frac{|(\nabla\rho) \times \boldsymbol{u}|}{\rho(\boldsymbol{r})|\boldsymbol{u}|} = c \tag{1}$$

where $\boldsymbol{u}$ is the local plasma flow vector. In Figure 7 we plot Equation (1) for $c = 0.03$ and $c = 0.06$, where we have used density per cm^3 and distances in astronomical units. Note that a smaller value of c results in a slightly broader contour that extends farther down the heliotail. Beyond ~1000 au down the heliotail the method fails when the density gradient across the HP becomes too small. While there will always be closed isosurfaces of temperature around the hot heliosphere embedded in the cool LISM (as shown in Figure 5), the isosurfaces of Equation (1) will not cross regions where the flow is parallel to a sharp gradient in density. From the plots in Figure 7 it is clear that all four models have outflow of SW from a single heliotail opening, even though they have not yet reached a true steady state.

Finally, in Figure 8 we show the steady-state heliosphere for Model IV, though configurations for Models I and II are very similar. It is clear from the figure that the Parker spiral field from the inner heliosphere convects down the heliotail where it allows faster flow through the centers of the "hoop" structure. We can also see that even though the flow down the center of the heliotail is slower, those streamlines still originate from the Sun, yielding a single elongated-SW outflow. Figure 8 also shows the connectivity of the plasma in the distant heliotail back to either the Sun, or the upstream LISM. For each pixel on a slice through the heliotail at $x = -1400$ au we traced the streamline backwards until we reach either the Sun, or the LISM upstream of the heliosphere. This process is similar to the level-set method in reverse and has the advantage that the result is strictly binary–either SW or LISM. Since the SW region in the plot for each of the models is contiguous, we can conclude that there is no mixing of SW and LISM plasmas in the tail. Instead the two flows will eventually reach an equilibrium mediated by charge-exchanging neutrals.

5. Discussion and Conclusions

We have used 3D MHD–neutral simulations of the SW–LISM interaction to investigate how such simulations reach a steady-state configuration. We looked at four models that started from different initial conditions, but utilized the same SW and LISM boundary conditions. The models couple the MHD equations for the ionized component to a particle MC approach for neutral hydrogen. The boundary conditions are

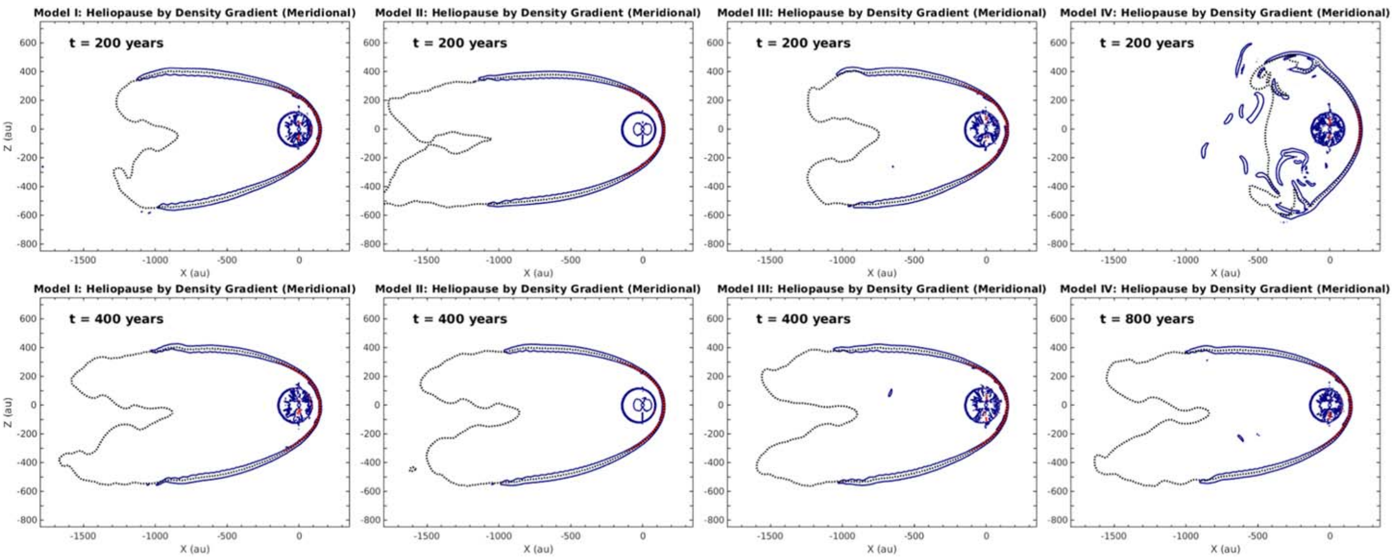

Figure 7. Illustration of the density gradient method (Equation (1)) for locating the HP, at $t = 200$ yr (top row) and once a steady state has been achieved (bottom row). Here we plot two contours ($c = 0.03$ in blue, and $c = 0.06$ in red) of the density gradient perpendicular to the plasma flow, along with the temperature contour $T = 100{,}000$ K (dotted).

time invariant, which leads to a steady-state solution for the heliosphere. We assumed a unipolar magnetic field for the SW, and set the LISM magnetic field to zero. These values were motivated by previous simulations that had resulted in an unusual "croissant" shape for the heliosphere, although in that case a fluid description for neutrals was used.

The simulations we considered reached a steady state by a relaxation approach, i.e., we solve the time-dependent equations until the time derivatives become effectively zero. While this is the commonly applied approach for time-invariant boundary conditions, the nature of the equations may introduce self-driven dynamics such as turbulence for which a truly invariant state does not exist. In addition to turbulence, the charge-exchange coupling may also introduce unstable dynamics. Because the charge-exchange rate is proportional to the plasma density, regions in the heliotail that have a slightly higher density will charge exchange more leading to enhanced cooling and compression, which enhances the charge-exchange rate further. This effect may be responsible for the ripples seen in Figure 2 for Model I. The longer neutral time step used in Model II reduces this effect, because the plasma and neutral timescales are not coupled.

For the four models considered, we assumed that the polarity of the SW magnetic field was the same in both the northern and southern hemispheres. This approach is sometimes used in simulations to prevent the formation of a flat current sheet, and/or the strong dissipation of magnetic field on scales of the grid. The use of a unipolar field means that the magnetic field in the "hoops" seen in the heliotail (Figure 8) spiral in the opposite sense for the northern and southern tubes. As a result, the field in the center of the heliotail is significantly stronger, because the fields add together. The stronger field perpendicular to the flow direction causes the flow through the middle of the heliotail to be slower than the flow through the hoop structures where the magnetic field is weaker. We note that the use of a bipolar field would likely reduce this effect (e.g., N. V. Pogorelov et al. 2015).

Our Model IV displays features of the "croissant"-shaped heliosphere reported by other authors (M. Opher et al. 2015), at least during the transition from a plasma-only steady state to a plasma–neutral steady state. In Model IV we include an additional population of neutrals in the initial condition. This case shows how additional structure in the initial condition may slow the convergence to a steady state, though importantly the eventual steady state is the same as for the other initial conditions we consider. In the evolution phase of Model IV we observed a "croissant" shape forming after about 200 yr, which then settled into the same steady state as the other models after 800 yr. These timescales depend on the size of the domain, and the extent, speed, and direction of the initial condition for the additional population of neutrals–effectively, the more sub-optimal the initial condition, the longer it takes to reach a steady state. One of the reasons Model IV develops a transient croissant shape is that the charge exchange of the additional population of neutrals ahead of the heliosphere creates ram pressure directed away from the heliosphere in the upstream LISM direction. This has the effect of pushing the maximum plasma pileup farther into the LISM, resulting in a more shallow density gradient from the HP into the LISM when compared to the other models. This ram pressure also has the effect of preventing the heliotail from getting longer, and instead allows the heliosphere to expand in the directions perpendicular to the LISM flow vector. Magnetic pressure in the SW results in the expansion being mostly in the polar directions. Eventually the additional population of neutrals introduced in the initial condition are depleted through charge exchange so that the ram pressure effect is removed, and the heliosphere settles into the same steady state as the other three models. It it interesting to note that the croissant-shaped heliosphere shown in M. Opher et al. (2020) also shows a pileup of LISM plasma significantly farther upstream of the HP than what is seen in our steady-state configurations (e.g., Figure 3). This suggests that a lack of ram pressure on the heliosphere may at least be partly responsible for their croissant shape. However, we do not claim here that the drivers of these two croissant-shaped heliospheres are the same.

In conclusion, we expect a heliosphere with a single tail to be the eventual steady state of the SW–LISM problem with

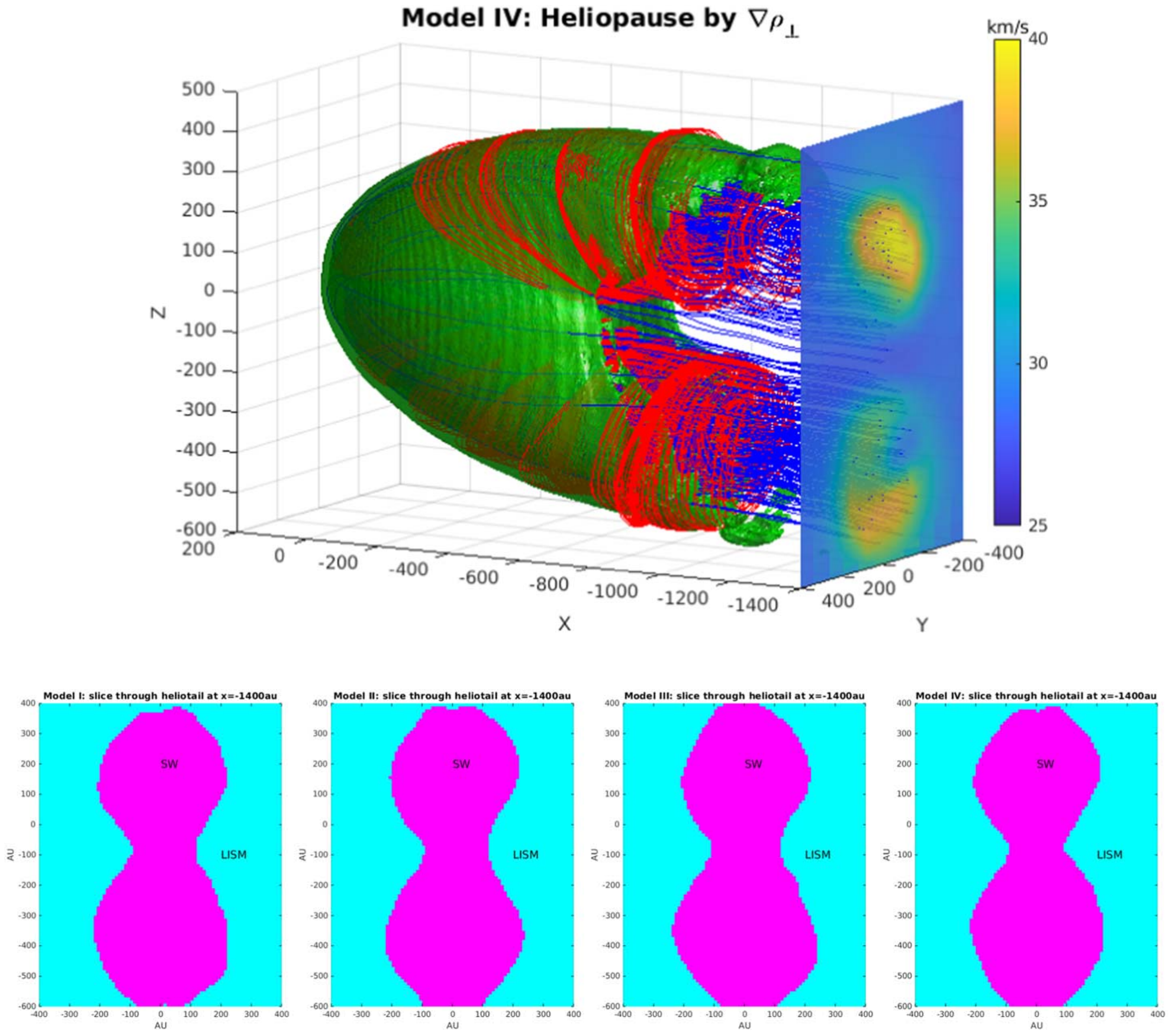

Figure 8. Steady-state heliosphere (at $t = 800$ yr) for Model IV showing HP surface (green), SW streamlines (blue), and SW magnetic field lines (red). Note that the field lines were generated using multiple starting locations designed to best indicate the hoop structure in the heliotail. The isosurface on the right side of the plot shows the plasma flow speed at $x = -1400$ au. The row of plots below represent the source of plasma that reaches $x = -1400$ au. Streamlines as traced backwards and plasma of solar origin is colored pink, while plasma from the LISM is colored cyan.

fixed boundary conditions, provided time-dependent effects such as turbulence are sufficiently suppressed. The final steady state does not depend on the initial conditions used, though some initial conditions will take longer to converge. Additionally, we may speed up the convergence to a steady-state solution by allowing the neutral component to evolve for a longer time than the plasma during plasma–neutral iterations, and unusual transient states may occur during the evolution to a steady state.

Acknowledgments

This work was supported by NASA grant 80NSSC24K0267. E.J.Z. acknowledges partial support from NASA's Heliophysics Supporting Research Program, through grant number 80NSSC21K1686. We also acknowledge the IBEX mission as part of NASA's Explorer Program (80NSSC18K0237).

ORCID iDs

Jacob Heerikhuisen https://orcid.org/0000-0001-7867-3633
Eric J. Zirnstein https://orcid.org/0000-0001-7240-0618
Nikolai V. Pogorelov https://orcid.org/0000-0002-6409-2392

References

Alexashov, D., & Izmodenov, V. 2005, A&A, 439, 1171
Bera, R. K., Fraternale, F., Pogorelov, N. V., et al. 2023, ApJ, 954, 147
Borovikov, S. N., Pogorelov, N. V., Burlaga, L. F., & Richardson, J. D. 2011, ApJL, 728, L21

Borovikov, S. N., Pogorelov, N. V., Zank, G. P., & Kryukov, I. A. 2008, ApJ, 682, 1404
Burlaga, L. F., & Ness, N. F. 2014, ApJL, 795, L19
Burlaga, L. F., Ness, N. F., Acuna, M. H., et al. 2005, Sci, 309, 2027
Burlaga, L. F., Ness, N. F., Acuna, M. H., et al. 2008, Natur, 454, 75
Decker, R. B., Krimigis, S. M., Roelof, E. C., et al. 2005, Sci, 309, 2020
Decker, R. B., Krimigis, S. M., Roelof, E. C., et al. 2008, Natur, 454, 67
Drake, J. F., Swisdak, M., & Opher, M. 2015, ApJL, 808, L44
Fraternale, F., Pogorelov, N. V., & Bera, R. K. 2023, ApJ, 946, 97
Golikov, E. A., Izmodenov, V. V., Alexashov, D. B., & Belov, N. A. 2017, MNRAS, 464, 1065
Gurnett, D. A., & Kurth, W. S. 2019, NatAs, 3, 1024
Gurnett, D. A., Kurth, W. S., Burlaga, L. F., & Ness, N. F. 2013, Sci, 341, 1489
Heerikhuisen, J., Florinski, V., & Zank, G. P. 2006, JGRA, 111, A06110
Heerikhuisen, J., & Pogorelov, N. V. 2010, in ASP Conf. Ser. 429, Numerical Modeling of Space Plasma Flows, Astronum-2009, ed. N. V. Pogorelov, E. Audit, & G. P. Zank (San Francisco, CA: ASP), 227
Heerikhuisen, J., Pogorelov, N. V., Florinski, V., Zank, G. P., & le Roux, J. A. 2008, ApJ, 682, 679
Heerikhuisen, J., Zirnstein, E. J., Funsten, H. O., Pogorelov, N. V., & Zank, G. P. 2014, ApJ, 784, 73
Izmodenov, V., Alexashov, D., & Myasnikov, A. 2005, A&A, 437, L35
Izmodenov, V. V., & Alexashov, D. B. 2015, ApJS, 220, 32
Izmodenov, V. V., & Alexashov, D. B. 2020, A&A, 633, L12
Kim, T. K., Pogorelov, N. V., Zank, G. P., Elliott, H. A., & McComas, D. J. 2016, ApJ, 832, 72
Kleimann, J., Dialynas, K., Fraternale, F., et al. 2022, SSRv, 218, 36
Kornbleuth, M., Opher, M., Baliukin, I., et al. 2021, ApJ, 923, 179
Korolkov, S., & Izmodenov, V. 2021, MNRAS, 504, 4589
Krimigis, S. M., Decker, R. B., Roelof, E. C., et al. 2019, NatAs, 3, 997
Kurth, W. S., & Gurnett, D. A. 2020, ApJL, 900, L1
Linde, T. J., Gombosi, T. I., Roe, P. L., Powell, K. G., & DeZeeuw, D. L. 1998, JGR, 103, 1889
McComas, D. J., Dayeh, M. A., Funsten, H. O., Livadiotis, G., & Schwadron, N. A. 2013, ApJ, 771, 77
McComas, D. J., Dayeh, M. A., Funsten, H. O., et al. 2018, ApJL, 856, L10
Michael, A. T., Opher, M., Tóth, G., Tenishev, V., & Borovikov, D. 2022, ApJ, 924, 105
Opher, M., Drake, J. F., Zieger, B., & Gombosi, T. I. 2015, ApJL, 800, L28
Opher, M., Drake, J. F., Zieger, B., Swisdak, M., & Toth, G. 2016, PhPl, 23, 056501
Opher, M., Loeb, A., Drake, J., & Toth, G. 2020, NatAs, 4, 675
Opher, M., Stone, E. C., & Liewer, P. C. 2006, ApJL, 640, L71
Osher, S., & Fedkiw, R. P. 2001, JCoPh, 169, 463
Parker, E. N. 1961, ApJ, 134, 20
Pauls, H. L., Zank, G. P., & Williams, L. L. 1995, JGR, 100, 21595
Pogorelov, N. V., Borovikov, S. N., Heerikhuisen, J., & Zhang, M. 2015, ApJL, 812, L6
Pogorelov, N. V., Borovikov, S. N., Zank, G. P., & Ogino, T. 2009, ApJ, 696, 1478
Pogorelov, N. V., Heerikhuisen, J., Roytershteyn, V., et al. 2017, ApJ, 845, 9
Pogorelov, N. V., & Matsuda, T. 1998, JGR, 103, 237
Pogorelov, N. V., Suess, S. T., Borovikov, S. N., et al. 2013, ApJ, 772, 2
Pogorelov, N. V., Zank, G. P., & Ogino, T. 2004, ApJ, 614, 1007
Pogorelov, N. V., Zank, G. P., & Ogino, T. 2006, ApJ, 644, 1299
Ratkiewicz, R., & Grygorczuk, J. 2008, GeoRL, 35, 23105
Richardson, J. D., Belcher, J. W., Garcia-Galindo, P., & Burlaga, L. F. 2019, NatAs, 3, 1019
Sternal, O., Fichtner, H., & Scherer, K. 2008, A&A, 477, 365
Stone, E. C., Cummings, A. C., McDonald, F. B., et al. 2005, Sci, 309, 2017
Stone, E. C., Cummings, A. C., McDonald, F. B., et al. 2008, Natur, 454, 71
Stone, E. C., Cummings, A. C., McDonald, F. B., et al. 2013, Sci, 341, 150
Tanaka, T., & Washimi, H. 1999, JGR, 104, 12605
Yu, G. 1974, ApJ, 194, 187
Zank, G. P. 1999, SSRv, 89, 413
Zirnstein, E. J., Heerikhuisen, J., McComas, D. J., et al. 2018, ApJ, 859, 104
Zirnstein, E. J., Heerikhuisen, J., Pogorelov, N. V., McComas, D. J., & Dayeh, M. A. 2015, ApJ, 804, 5
Zirnstein, E. J., Heerikhuisen, J., Zank, G. P., et al. 2017, ApJ, 836, 238
Zirnstein, E. J., Shrestha, B. L., McComas, D. J., et al. 2022, NatAs, 6, 1398